Absorption and Emission Spectra of Impurities in Solids

C. Stuart Kelley
Physical Research Division, Edgewood Arsenal, Maryland 21010
(Received 15 May 1972)

Absorption and emission line shapes are calculated for impurities that couple to the lattice through an interaction containing both linear and quadratic terms. Specific examples of absorption-band shapes are computed for temperatures at and well above 0 K, and are compared to band shapes for the limiting cases of linear interaction and quadratic interaction. The strength of the quadratic-interaction parameter is shown to influence the shape, and thereby the observation, of zero-phonon lines; the temperature dependence of the over-all spectral-band shape; and the symmetry of the absorption and emission spectra. From the temperature dependence of the absorption-band shape observed experimentally, values of the linear- and quadratic-interaction parameters can be estimated.

I. INTRODUCTION

Electronic transitions within impurities in solids are quite strongly affected by lattice vibrations. In addition to the sharp absorption and emission lines due to the purely electronic (zero-phonon) transitions, phonon-assisted transitions also introduce absorption and emission bands. These phonon-assisted transitions produce smooth broad bands in one-impurity-lattice system, and quite irregularly shaped bands in another.

To predict absorption and emission spectra, the most widely used, and the simplest, approximation to the impurity-lattice interaction, the linear interaction, has been used. It has been applied to the interpretation of both smoothly and irregularly shaped phonon-assisted bands. The semiclassical approximation[1-4] is successful in fitting the smooth broad absorption- and emission-band shapes. The quantum-mechanical treatment, with linear interactions,[5,6] has been applied to predict the structural nature of the broad bands, and the transition from smoothly to irregularly shaped bands.[7]

For impurities at sites of inversion symmetry, the linear interaction vanishes for odd-parity vibrational modes, and interaction terms that are quadratic dominate. The quantum-mechanical treatment of the quadratic interaction[8] has been used in the interpretation of the absorption spectra of a few specific impurity systems,[9,10] and explains the structural nature of the broad band and the temperature dependence of the zero-phonon line.

In a recent paper, Mostoller *et al.*[11] have extended the convolution approach of Ritter[5] to fit the experimental phonon-assisted absorption spectrum at $T=0$ of the N_1 color center in NaCl using a self-consistent one-phonon density of states. This method has not yet been applied to systems at nonzero temperatures.

The present approach is to include both linear- and quadratic-interaction terms to predict absorption- and emission-band shapes at nonzero temperatures. Despite its complexity, this general interaction has the potential for widest application. The procedure is to review the theory of line shapes for absorption and emission, compute representative examples, compare these to the line shapes in the limiting cases of linear and quadratic interactions, and provide methods for estimating values of the linear- and quadratic-interaction parameters from experimental band shapes.

II. LINE-SHAPE THEORY

The line shape for electric-dipole transitions from the electronic ground state a (wave function Ψ_a) to the electronic excited state b (wave function Ψ_b) of the impurity is proportional to the sum over the initial and final states of

$$\langle \Psi_a | e\vec{r} | \Psi_b \rangle^2 \, \delta(E - E_b + E_a) \, ,$$

where the initial states must be weighted in accordance with Boltzmann statistics. The δ function involving the energies of the ground and excited states locates the transition energy. The electric-dipole operator is $e\vec{r}$.

The Hamiltonian describing the interaction between the impurity and the lattice is

$$H = T_N + U_N + T_E + U_E + U_{E,N} \, ,$$

where the kinetic energy operator for nuclei is T_N, and that for electrons is T_E. The interactions among the nuclei are described by U_N, those among the electrons are by U_E. Electron-nuclei interactions are described by $U_{E,N}$. For fixed nuclei, the Hamiltonian reduces to the electronic part of the Hamiltonian $H_E = T_E + U_E + U_{E,N}$, where $H_E \Psi = \epsilon_E \Psi$. A separation of variables is affected by assuming a product wave function, $\Psi = \Phi(\vec{r}_l, \vec{R}_l) \times \chi(\vec{R}_l)$, where the $\vec{r}_l$ denote all electron positions, and $\vec{R}_l$ all the nuclear positions. Then

$$H\Psi = T_N \Phi\chi + U_N \Phi\chi + \epsilon_E \Phi\chi = \epsilon \Phi\chi \, . \quad (1)$$

Denoting the nuclear mass as M,

$$T_N\Phi\chi=\sum_l \frac{-\hbar^2}{2M}(\nabla_{R_l}^2\Phi\chi)$$
$$=\sum_l\frac{-\hbar^2}{2M}[(\nabla_{R_l}^2\Phi)\chi+2(\nabla_{R_l}\Phi)(\nabla_{R_l}\chi)+\Phi\nabla_{R_l}^2\chi]. \quad (2)$$

The second term on the right-hand side represents the second-order effect of electron-phonon interactions, and is neglected (the adiabatic approximation). The third term on the right-hand side of Eq. (2) is neglected because electrons are periodic throughout the lattice and accompany the nuclei: $\Phi(\vec{r})=\Phi(\vec{r}-\vec{R})$. Thus $\nabla_{R_l}=-\nabla_{r_l}$, and

$$\frac{-\hbar^2}{2M}\Phi\nabla_{R_l}^2\chi=\frac{m}{M}\frac{\hbar^2}{2m}\Phi\nabla_{r_j}^2\chi\ ,$$

which is of the same form as a term in $T_E=\sum(-\hbar^2/2m)\nabla_{r_j}^2$ but smaller by the ratio of the electron mass m to the nuclear mass M ($\sim 10^{-5}$). Accordingly it is neglected. Defining an effective potential, $V_e=U_N+\epsilon_E$, Eq. (1) becomes

$$\left(\sum_l\frac{-\hbar^2}{2M}\nabla_{R_l}^2+V_e\right)\chi=\epsilon\chi\ .$$

Expanding V_e for the ground state of the electronic transition in a power series in the displacements of the nuclei from their equilibrium positions, and performing a normal-mode transformation:

$$V_{ea}=\sum_l\tfrac{1}{2}\omega_{la}^2q_l^2\ .$$

The normal coordinates are q_l and the frequency is ω_{la}. Then

$$\sum_l\left(\frac{-\hbar^2}{2}\frac{\partial^2}{\partial q_l^2}+\tfrac{1}{2}\omega_{la}^2q_l^2\right)\chi_a=\epsilon_a\chi_a\ .$$

Solutions are $\chi_a=\Pi_l\chi_{la}(q_l)$, where the χ_{la} satisfy

$$\left(-\frac{\hbar^2}{2}\frac{\partial^2}{\partial q_l^2}+\tfrac{1}{2}\omega_{la}^2q_l^2\right)\chi_{la}(q_l)=\epsilon_{la}\chi_{la}(q_l)$$

and are harmonic-oscillator wave functions. The adiabatic effective potential V_{eb} for the excited state of the transition is written as a series expansion in terms of the ground-state normal coordinates:

$$V_{eb}=E_0+\sum_l a\hbar\omega_{lb}(\omega_{lb}/\hbar)^{1/2}q_l+\sum_l\tfrac{1}{2}\omega_{lb}^2q_l^2+\sum_{l\neq j}V_{lj}q_lq_j+\cdots\ .$$

The last term written above and terms following it are neglected. The solutions are $\chi_b=\Pi_l\chi_{lb}(q_l)$, where the $\chi_{lb}(q_l)$ satisfy

$$\left\{\frac{-\hbar^2}{2}\frac{\partial^2}{\partial q_l^2}+\left[\left(\frac{\omega_{lb}^2}{2}\right)^{1/2}q_l+a\left(\frac{\hbar\omega_{lb}}{2}\right)^{1/2}\right]^2\right\}\chi_{lb}=\left(\frac{\epsilon_{lb}-E_0+a^2\hbar\omega_{lb}}{2}\right)\chi_{lb}.$$

The χ_{lb} are harmonic-oscillator wave functions having displaced equilibria, and frequencies that differ from those of the ground state. In terms of the quadratic-interaction parameter, $R=\omega_b/\omega_a$, and the linear-interaction parameter a and dropping the subscript l,

$$\chi_{ai}=(A/\pi^{1/2}2^i i!)^{1/2}\,e^{-A^2q^2/2}H_i(Aq)\ ,$$
$$\chi_{bf}=(AR^{1/2}/\pi^{1/2}2^f f!)^{1/2}e^{-(R^{1/2}Aq+a)^2}\times H_f(R^{1/2}Aq+a)\ ,$$

where $A=(\omega_a/\hbar)^{1/2}$, the $H_n(x)$ are Hermite polynomials, and i and f denote the vibrational quantum numbers of the ground and excited states, respectively. The matrix elements necessary for computation of the line shapes are

$$\langle\Psi_a|e\vec{r}|\Psi_b\rangle=\langle\Phi_a|e\vec{r}|\Phi_b\rangle\langle\chi_{ai}|\chi_{bf}\rangle\ .$$

Eigenvalues of the ground state are $\epsilon_a=(i+\frac{1}{2})\hbar\omega$, and eigenvalues of the excited state are $\epsilon_b=E_0-a^2R\hbar\omega/2+(f+\frac{1}{2})R\hbar\omega$. The transition $i\rightarrow f$ ($i\rightarrow f$ denotes absorption, $i\leftarrow f$ emission) is located by a δ function involving the difference in energy of the ith vibrational level of the ground state and the fth vibrational level of the excited state,

$$\delta(E-E_0-[R(1-a^2)-1]\hbar\omega/2-(Rf-i)\hbar\omega)\ .$$

The population probability of the ith vibrational level of the initial state of the transition is $n_i/n_0=e^{-\Delta\epsilon_i/kT}$, where $\Delta\epsilon_i$ is the energy difference between the ith and the zeroth vibrational levels, k is the Boltzmann constant, and T is the temperature. For a system of n ions, n_i are in the ith vibrational state and n_0 are in the zeroth vibrational state. The population probability for the ith level is

$$n_i/n=e^{-\Delta\epsilon_i/kT}\Big(\sum_{j=0}^{\infty}e^{-\Delta\epsilon_j/kT}\Big)^{-1}\ .$$

For absorption $\Delta\epsilon_i=i\hbar\omega$, so

$$n_i/n=e^{-i\theta/T}\Big(\sum_{j=0}^{\infty}e^{-j\theta/T}\Big)^{-1}=e^{-i\theta/T}(1-e^{-\theta/T})\ ,$$

where $\theta=\hbar\omega/k$. For emission, $\Delta\epsilon_f=fR\hbar\omega$, and

$$n_f/n=e^{-fR\theta/T}(1-e^{-R\theta/T})\ .$$

Because the wave functions are real, $\langle\chi_{ai}|\chi_{bf}\rangle=\langle\chi_{bf}|\chi_{ai}\rangle$. An expression for $\langle\chi_{ai}|\chi_{bf}\rangle=M_{if}$ has been given,[12] however, a somewhat more tractable expression is

$$M_{if}=(-1)^f\left(\frac{2^{i+f+1}R^{i+1/2}i!f!}{(1+R)}\right)^{1/2}[a/(1+R)]^{i+f}\times e^{-a^2/2(1+R)}\sum_{l=0}^{i+f}\left(\frac{1+R}{-a^2}\right)^l(l!)^{-1}\sum_{j=0}^{(i-l)/2}\left(\frac{1-R^2}{4a^2R}\right)^j\times\frac{1}{j!(i-l-2j)!}\sum_{k=0}^{(f-l)/2}\left(\frac{1-R^2}{-4a^2}\right)^k\Big/k!(f-l-2k)! \quad (3)$$

and the sum over l is to either i or f, whichever is smaller. This expression reduces to that for linear interactions if $R=1$ and to that for quadratic interactions if $a=0$. Expressions for M_{if} for these cases are given elsewhere.[8,13] The absorption (or emission) intensity is the sum over initial and final states of the products of the squares of the matrix elements for the transitions, the population probabilities for the initial levels, and the δ functions that locate the transitions:

$$I_\alpha(E,T)=K_\alpha C_{ab}^2(1-e^{\theta/T})\sum_{i,f} M_{if}^2 e^{-i\theta/T} \times \delta(E-E_0-[R(1-a^2)-1]\hbar\omega/2-(Rf-i)\hbar\omega) \quad (4)$$

and

$$I_\epsilon(E,T)=K_\epsilon C_{ba}^2(1-e^{-R\theta/T})\sum_{i,f} M_{if}^2 e^{-fR\theta/T} \times \delta(E-E_0-[R(1-a^2)-1]\hbar\omega/2-(Rf-i)\hbar\omega), \quad (5)$$

where K_α and K_ϵ are constants, and $C_{ab}=\langle\Phi_a|e\vec{r}|\Phi_b\rangle$ and $C_{ba}=\langle\Phi_b|e\vec{r}|\Phi_a\rangle$.

III. CALCULATIONS AND DISCUSSION

Because $M_{if}=M_{fi}$, the absorption spectrum, Eq. (4), and the emission spectrum, Eq. (5), near $T=0$ are virtually exact mirror images about the zero-phonon line provided that $R=1$. This symmetry near $T=0$ is broken for $R\neq1$ by the dissimilar line spacings. This behavior persists, with modifications, when T is not near zero. Then the absorption and emission spectra are again symmetric about the zero-phonon line provided that $R=1$. For $R\neq1$, the symmetry is broken for two reasons: the dissimilar line spacings and the dissimilar thermal population factors. The unequal thermal population factors indicate symmetry (disregarding for the moment the dissimilar line spacings) of the absorption spectrum at temperature T and the emission spectrum at temperature RT. Even so, the emission spectrum is broader or narrower than the absorption spectrum accordingly as R is less than or greater than unity—a direct consequence of the dissimilar line spacings. Because calculation of the emission spectrum is virtually the same as that for the absorption spectrum, the following discussion is limited to the absorption spectrum.

Absorption spectra were calculated from Eq. (4), with M_{if} given by Eq. (3). The calculations included contributions from $0\leq i,\ f\leq 26$, which amply illustrate the features of the spectra. Results of the calculations are presented in the figures, which were drawn from the computer print out. The computer print out consisted of a series of spikes for each value of i, any one series having a smooth envelope. The resulting spectrum, composed of a multitude of sharp spikes, is difficult to present in graphical form. In any physical system, the transitions will have nonzero widths due to deviations from the approximations used in Sec. II. Also, the finite bandpass of the spectrometer recording these spectra will induce effective line broadening. Thus, within each i envelope, the contributions of the spikes to the total spectrum will tend to assume the shape of the envelope. Accordingly, each spectrum presented in the figures is the sum of the i envelopes. Figure 1 shows this construction of the total-absorption-band shape from the envelopes.

Each spectrum in the figures is characterized by values for R, a, and T/θ. The ordinates of the figures are $P_\alpha=I_\alpha/K_\alpha C_{ab}^2$, and the abscissas

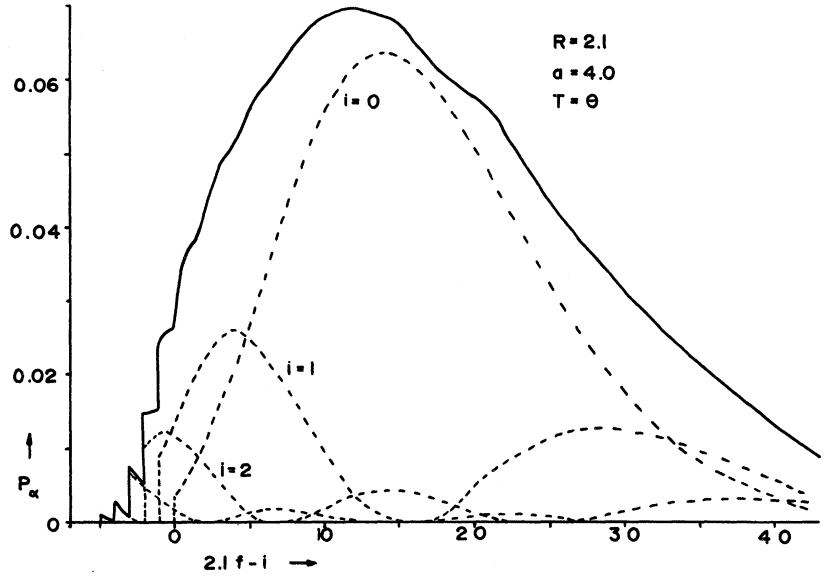

FIG. 1. P_α (proportional to optical absorption) versus $2.1f-i$ (proportional to energy) at $T=\theta$ for $R=2.1$ and $a=4.0$ (solid line). Contributions to the band from the i envelopes are shown by dashed lines. The $i=0$ envelope is, except for being diminished by the factor $(1-e^{-1})$, the $T=0$ spectrum.

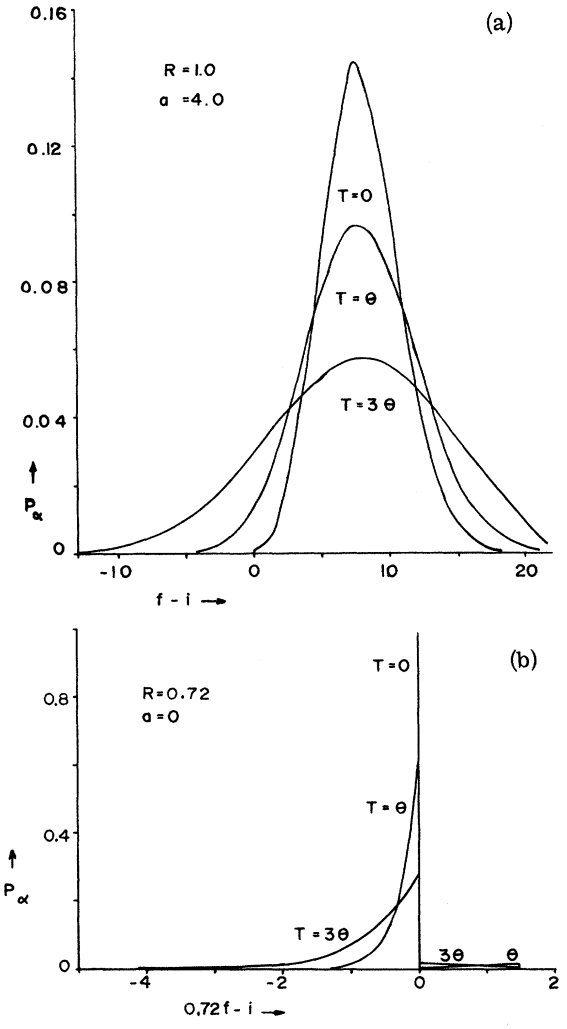

FIG. 2. P_α (proportional to optical absorption) versus energy for the two limiting cases. (a) The limiting case of linear interaction, with $a=4.0$ at $T=0$, θ, and 3θ. The abscissa $f-i$ is proportional to energy. (b) The limiting case of quadratic interaction, with $R=0.72$ at $T=0$, θ, and 3θ. The abscissa $0.72f-i$ is proportional to energy.

are $K=Rf-i=(E-E_0)\hbar\omega-\frac{1}{2}[R(1-a^2)-1]$. For many systems, θ is on the order of 100 K, so that $T=0$, θ, 3θ correspond roughly to liquid-helium, liquid-nitrogen, and room temperatures. Before proceeding to spectra due to the presence of both linear and quadratic interaction terms, it is useful to review the limiting cases of linear ($R=1$) and quadratic ($a=0$) interactions.

The spectrum for linearly interacting systems with $a=4.0$ is given in Fig. 2(a). The low-temperature ($T=0$) spectrum is roughly Gaussian shaped, but has a low-energy cutoff at the zero-phonon line. As the temperature is raised, the band broadens, decreases in peak intensity, and the maximum does not shift appreciably in energy. The zero-phonon transition is now superposed on all $i\to f=i$ transitions, and is lost in the low-energy tail, which is longer than the high-energy tail. The structural nature of the spectrum is, however, essentially unchanged.

The spectrum for quadratically interacting systems with $R=0.72$ [Fig. 2(b)] at $T=0$ is dominated by the zero-phonon line, in contrast to the spectrum for the linear interaction case (except when a is quite small, in which case[11] the spectrum consists primarily of the zero-phonon line and the one-phonon-assisted line). The zero-phonon line is the low-energy cutoff. At $T>0$, the spectrum is essentially an asymmetric low-energy (for $R<1$) or high-energy (for $R>1$) band, having a sharp drop in intensity at the zero-phonon line, which is located at the band maximum.

Spectra for systems having both linear and quadratic interaction terms are shown in Figs. 1, 3, and 4. The zero-phonon line is the low-energy cutoff for the Gaussian-shaped $T=0$ band, and decreases in intensity with increasing a, reflecting the decreasing overlap of the wave functions. If a is large, the peak of the band occurs for large f, and differentiation of Eq. (4) locates the peak of the spectrum at

$$K_m=Rf-i\simeq[2a^2/(1+R)^2]\,e^{-2(1-R)/(1+R)}$$

This reduces to $K_m=0$ for the quadratic case and to that reported[8] for the linear case, $K_m=a^2/2$. The peak of the band shifts to higher energy, away from the zero-phonon line, with increasing a [from Figs. 2(b), 3(a), and 3(b), it can be seen that K_m increases linearly with a^2], and also with increasing R [Figs. 1, 2(a), and 4]. The band shape at $T=0$ is skewed to the high-energy side for $R>1$, and to the low-energy side for $R<1$.

As the temperature increases, the high-energy side of the band becomes more uniformly smoothed than the low-energy side, which develops structure. The band broadens and decreases in maximum intensity. Broadening occurs predominantly on the low-energy side and obscures the location of the zero-phonon line, producing a low-energy tail for $R<1$, and a high-energy tail for $R>1$. The skewness of the $T=0$ spectrum and the changing shape of the spectrum with temperature provide a method for estimating the value of the quadratic interaction parameter from experimental data.

The composition of the spectrum for $R=2.1$, $a=4.0$, at $T=\theta$ is shown in Fig. 1. The spectrum is composed of i envelopes, whose intensities decrease with increasing i due to the thermal population of the initial levels. The $i=1$ double-peaked envelope is centered to the high-energy side of the peak of the $i=0$ envelope, thus contributing

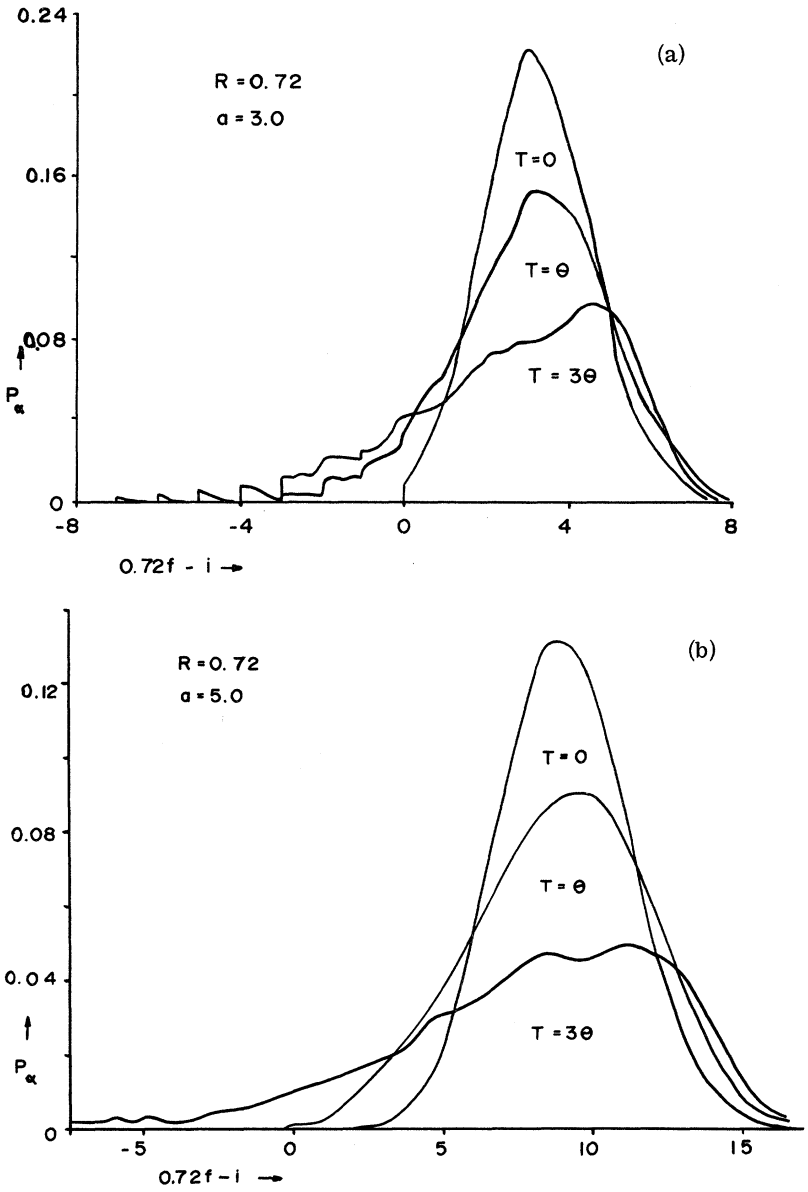

FIG. 3. P_α (proportional to optical absorption) versus $0.72f-i$ (proportional to energy) with $R=0.72$ at $T=0$, θ, and 3θ for (a) $a=3.0$ and (b) $a=5.0$. The low-energy cutoff for the $T=0$ spectra occur at $0.72f-i=0$. The position of the peak of the spectrum increases linearly with a^2.

to the high-energy tail. Because the low-energy peaks of the $i\neq 0$ envelopes are intense, they provide the structure in the low-energy side of the total band shape.

At $T=0$, both weakly quadratic ($R\simeq 1$) and strongly quadratic ($R\neq 1$) systems have narrow zero-phonon lines because only the $i=0$ level is populated. However, for a given value of a, the strongly quadratic zero-phonon line is more intense than the weakly quadratic zero-phonon line. For weakly quadratic systems at $T>0$, the $i\rightarrow f=i$ transitions very nearly coincide in energy, producing an unresolved zero-phonon line that is, for a given value of a, less intense and narrower than if $R\simeq 1$. Thus, the zero-phonon line will be observed experimentally with more difficulty for weakly quadratic systems than for strongly quadratic ones.

Because the zero-phonon line is weak in systems for which a is large (the overlap of the $i=0$ and $f=0$ wave functions decreases with increasing a), the observation of zero-phonon lines in the experimental spectra facilitates an estimate for the value of the linear-interaction parameter.

When $R\simeq 1$ and a is small, the zero-phonon line is intense and displays a temperature-dependent half-width. This temperature dependence arises from inclusion of the quadratic interaction, as previously reported.[11] Then the $i\rightarrow f=i$ transitions cluster closely and are the most intense lines

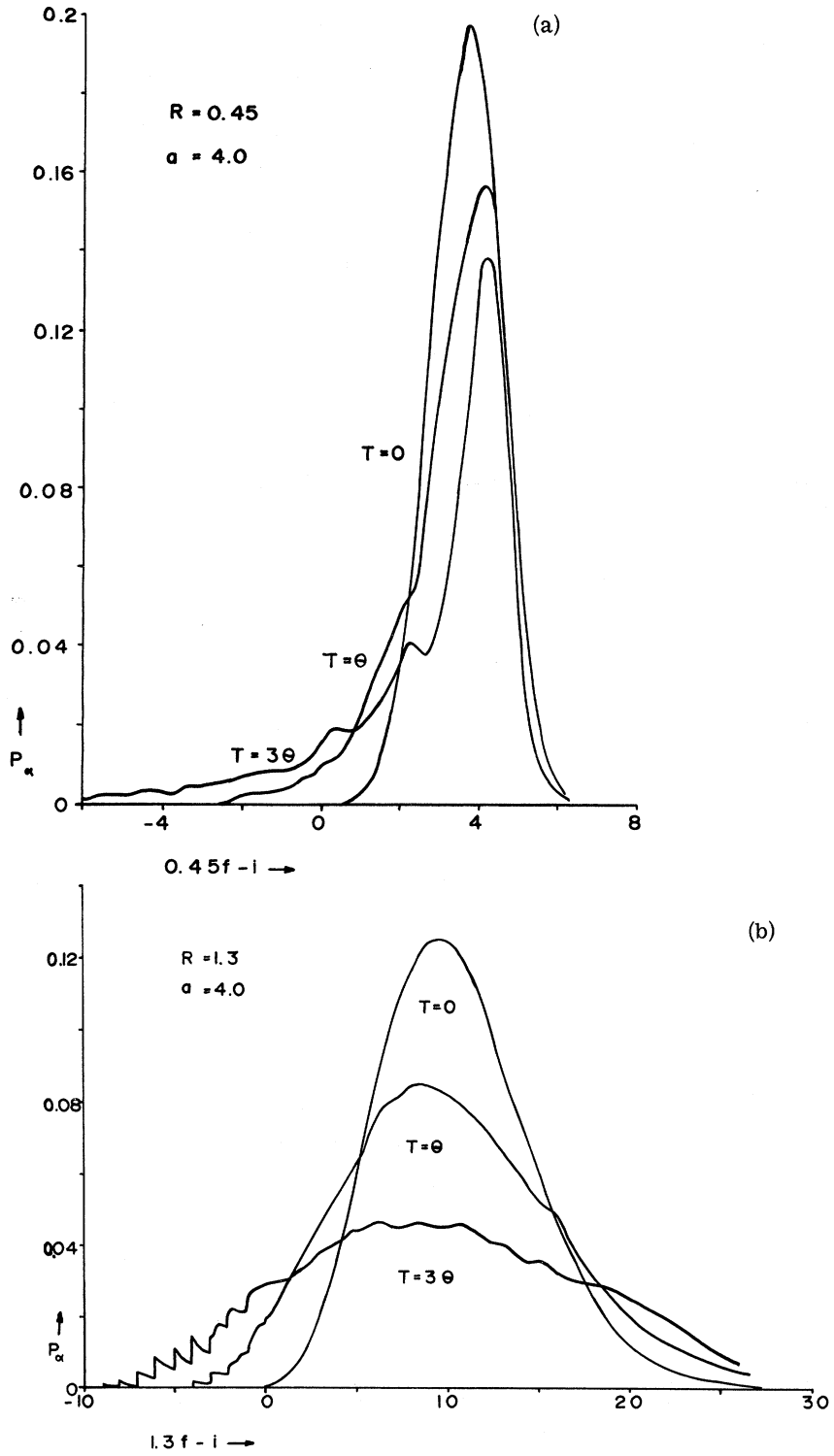

FIG. 4. P_α (proportional to optical absorption) versus energy with $a=4.0$ at $T=0$, θ, and 3θ. The $T=0$ spectrum is skewed to low energy for $R<1$ [(a) with $R=0.45$] and to high energy for $R>1$ [(b) with $R=1.3$].

(because the overlap of the wave functions is greatest for these transitions).

IV. CONCLUSIONS

The impurity-lattice interaction that includes both linear and quadratic terms has not been treated in detail for $T=0$, and not at all for $T>0$, and was therefore chosen for this investigation. The theory of absorption and emission line shapes is reviewed, and specific examples of the spectra are presented. Although the resulting spectra are

similar to those for linearly interacting systems, there are notable differences that depend on the strength of the quadratic-interaction parameter. These are the shape and resolution of the zero-phonon line; the temperature dependence and, to a lesser extent, the shape of the broad band; the occurrence of mirror symmetry of the low-temperature absorption and emission spectra; and the relation of the high-temperature absorption and emission spectra. From the temperature dependence of the shape of broad band and the observation of zero-phonon lines, values of the linear- and quadratic-interaction parameters can be estimated from experimental spectra.

ACKNOWLEDGMENT

The author is appreciative for the computer program drawn up by T. W. Crimmins for computation of the line intensities.

[1]F. E. Williams, J. Chem. Phys. 19, 457 (1951).
[2]F. E. Williams and M. H. Hebb, Phys. Rev. 84, 1181 (1951).
[3]F. E. Williams, Phys. Rev. 82, 281 (1951).
[4]M. Lax, J. Chem. Phys. 20, 1752 (1952).
[5]J. T. Ritter, J. Chem. Phys. 53, 3461 (1970).
[6]J. T. Ritter and J. J. Markham, Phys. Rev. 185, 1201 (1969).
[7]J. J. Markham, Rev. Mod. Phys. 31, 956 (1959).
[8]T. H. Keil, Phys. Rev. 140, A601 (1965).
[9]T. H. Keil and A. Gold, Phys. Rev. 140, A906 (1965).
[10]C. S. Kelley and F. E. Williams (unpublished).
[11]M. Mostoller, B. N. Ganguly, and R. F. Wood, Phys. Rev. B 4, 2015 (1971).
[12]J. B. Coon, R. E. DeWames, and C. M. Loyd, J. Mol. Spectroscopy 8, 285 (1962).
[13]C. S. Kelley, Edgewood Arsenal Technical Report No. 4575, 1971 (unpublished).

PHYSICAL REVIEW B VOLUME 6, NUMBER 11 1 DECEMBER 1972

Relaxation of Local-Moment Nuclei in Metals

R. E. Walstedt
Bell Laboratories, Murray Hill, New Jersey 07974
and
A. Narath
Sandia Laboratories, Albuquerque, New Mexico 87115
(Received 27 April 1972)

Relaxation processes for the nuclei of dilute S-like local moments in metals are investigated using both perturbation and dynamic-susceptibility techniques. In contrast to host nuclear relaxation, terms analogous to the Benoit–de Gennes–Silhouette (BGS) and Giovannin–Heeger (GH) processes are obtained in the local case by working only to second order in J_{sd}. The two methods of calculation are found, using the dynamic susceptibilities of Götze and Wölfle, to agree exactly within the approximations used. Contrary to the traditional view, the BGS process is found to consist of both real and virtual local-moment-excitation terms, becoming a purely *virtual* mechanism for large H_0/T. The GH process appears as an interference effect between the first-order (Korringa) term and the virtual BGS term. A similar relationship is believed to hold in the host-relaxation case. The local T_2 is found to behave rather differently from T_1 at low temperatures, with T_1 and T_2 merging into a single isotropic field-independent rate for sufficiently small H_0/T. The present calculations provide a qualitative understanding of the AgMn:^{55}Mn saturation results given by Okuda and Date.

I. INTRODUCTION

The relaxation of bulk metal nuclei by relatively dilute local moments has by now been studied quite extensively, both in terms of theory[1–4] and experiment.[5–8] In this paper we investigate the related question of relaxation processes for the local-moment nuclei themselves in such systems, e.g., of the ^{55}Mn nuclei in dilute CuMn or AgMn. It will be seen that such nuclear relaxation processes can be very rapid. Our first objective in calculating their strength is to determine under what conditions one might hope to apply the powerful methods of pulsed NMR to the observation of these resonances.

The motivation for such experiments is similar to that for the host-relaxation measurements, namely, to study the fluctuation properties of dilute moments in metals. On this basis the local-moment nuclear relaxation has the advantages of (a) being, in general, much larger than the background Korringa rate and (b) avoiding the difficult questions of host-hyperfine-coupling strength, spatial averages of relaxation-rate contributions,